

Ultrasound



1 Ultrasound

Ultrasound is a sound wave with a frequency greater than the upper limit of the human hearing range. In contrast to electromagnetic waves, sound waves need a medium to propagate (gases, liquids, or solids). Ultrasound is thus not separated from normal sound based on differences in physical properties, but only by the fact that humans cannot hear it. Although this limit varies from person to person, commonly sound frequencies larger than 20kHz are called ultrasound. Ultrasound is used in many different fields. Ultrasonic devices are used to detect objects and measure distances. Ultrasonic imaging (sonography) is used in medicine. Animals such as bats use ultrasound to navigate in darkness.

In physics the elastic constants of solids can be investigated by measuring the velocity and attenuation of a transmitted ultrasound wave. This yielded significant progress in understanding the interactions between electrons and the atomic lattice. There is essentially no difference between thermal motion (random vibrations) and elastic waves. With the aid of ultrasonic waves (wavelength of about $\lambda = 1\text{cm}$), it is possible to get information on the order of the mean free path of the electrons in solids (especially in metals). At low temperatures ($T < 200\text{K}$) the phonons (quantized lattice vibrations) slowly “freeze” so that the mean free path of the electrons increases. At these low temperatures the sound attenuation is mainly dominated by the free electrons. Thus, at low temperatures it becomes possible to study the behavior of electrons and especially the interactions with the atomic lattice. In addition, there is the opportunity to study phase transitions in the material using ultrasonic waves. For example the phase transition of a normal conductor to a superconductor at T_c leads to a recombination of the free electrons into Cooper pairs. As a result the contribution of the free electrons to the sound attenuation vanishes completely. Therefore it is possible to investigate the phase transition to the superconductor phase of a material by measuring the sound attenuation.

This lab course experiment will give a first insight into ultrasound measurement techniques and the appropriate electronic setup.

2 Theoretical Background

2.1 Hooke's Law

As far back as the 17th century Robert Hooke (1635-1703) recognized that stress σ (force F per area A) is proportional to the strain ε (change of the length per length):

$$\sigma = E \cdot \varepsilon,$$
$$\varepsilon = \frac{\Delta L}{L} \quad \sigma = \frac{F}{A}$$

where the constant E denotes Young's modulus (also called the elastic modulus). In the case of an atomic lattice the validity of Hooke's law is surprising because of the nonlinear nature of atomic interactions. However, since only a small strain is considered, it is possible to linearize the interaction force by a Taylor approximation.

A macroscopic solid state body does not respond to a certain strain with stress in the exactly opposite direction (see Fig.2.1).

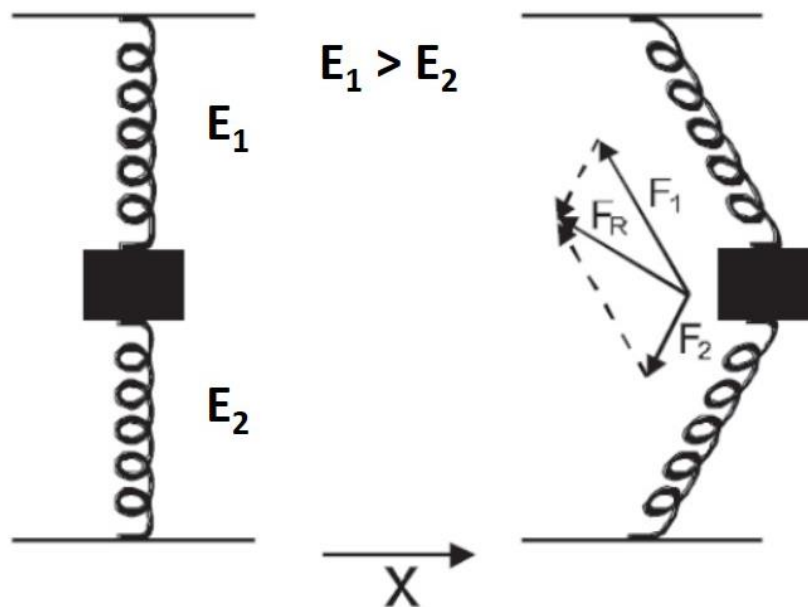


Fig. 2.1: A macroscopic object may not necessarily respond to a strain with stress in precisely the opposite direction.

A simple model may illustrate this: Applying a strain to a spring system in x-direction (see Fig. 2.1) will result in a responsive force which is given by the vector sum of the two spring forces. This force is no longer pointing in exactly the opposite direction to the strain. To extend Hooke's law to a solid this change of direction must be considered. Therefore the linear Hooke's law must be modified so that strain and

stress described by a tensor of 4th order. Fig. 2.2 illustrates the components of the strain tensor. Three different directions of strain forces can be applied to the three different surfaces of the cubic, thus resulting in 9 components of the strain tensor $\underline{\underline{\sigma}}$.

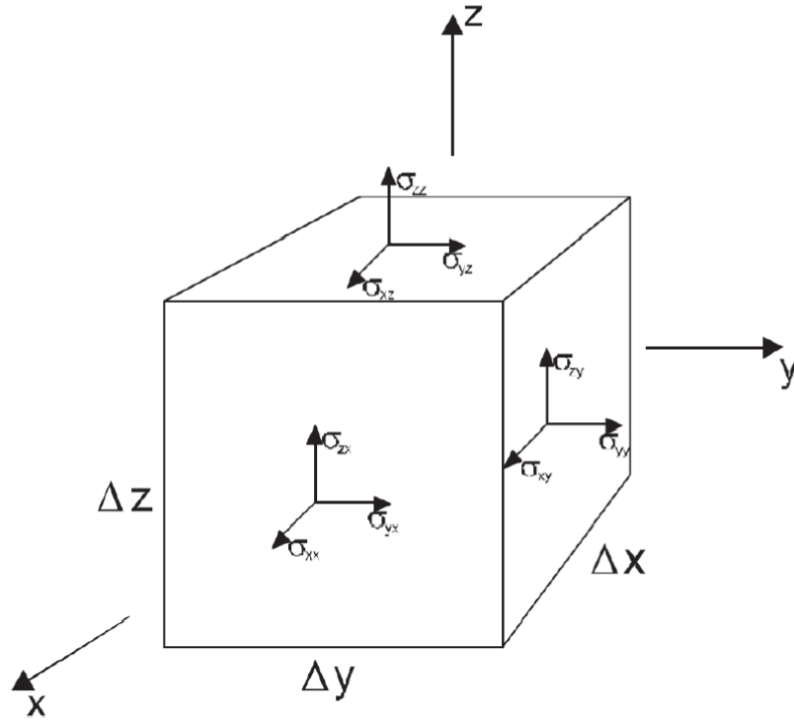


Fig. 2.2: Illustration of the matrix elements of the strain tensor.

$$\underline{\underline{\sigma}} = \underline{\underline{E}} \bullet \underline{\underline{\varepsilon}}$$

$$\underline{\underline{\sigma}} = \begin{pmatrix} \sigma_{xx} & \sigma_{xy} & \sigma_{xz} \\ \sigma_{yx} & \sigma_{yy} & \sigma_{yz} \\ \sigma_{zx} & \sigma_{zy} & \sigma_{zz} \end{pmatrix}, \underline{\underline{\varepsilon}} = \begin{pmatrix} \varepsilon_{xx} & \varepsilon_{xy} & \varepsilon_{xz} \\ \varepsilon_{yx} & \varepsilon_{yy} & \varepsilon_{yz} \\ \varepsilon_{zx} & \varepsilon_{zy} & \varepsilon_{zz} \end{pmatrix}$$

Since each element of the stress tensor should be connected to each element of the strain tensor, $\underline{\underline{E}}$ has $9 \times 9 = 81$ elements. The elements of the tensor, which are also referred to as elastic moduli, thus have 4 indices. Since the strain and stress tensor has 6 linearly independent elements the resulting $\underline{\underline{E}}$ tensor has only $6 \times 6 = 36$ linearly independent elements:

$$\underline{\underline{E}} = \begin{pmatrix} E_{xxxx} & E_{xxyy} & E_{xxzz} & E_{xxyz} & E_{xxxz} & E_{xxxxy} \\ E_{yyxx} & E_{yyyy} & E_{yyzz} & E_{yyyz} & E_{yyxz} & E_{yyxy} \\ E_{zzxx} & E_{zzyy} & E_{zzzz} & E_{zzyz} & E_{zzxz} & E_{zzxy} \\ E_{yzxx} & E_{yzyy} & E_{yzzz} & E_{yzyz} & E_{yzxz} & E_{yzyx} \\ E_{xzxx} & E_{xzyy} & E_{xzzz} & E_{xzyz} & E_{xzxz} & E_{xzxy} \\ E_{xyxx} & E_{xyyy} & E_{xyzz} & E_{xyyz} & E_{xyxz} & E_{xyxy} \end{pmatrix}$$

From symmetry considerations the number of linearly independent elements further decreases to 21 elements. In addition, considering only cubic crystal structures 3 linearly independent elements remain (E_{xxxx} , E_{xxyy} , E_{yzyz}). For simplification reasons

the indices are defined as follows (Voigt notation): $xx=1$, $yy=2$, $zz=3$, $yz=4$, ($xz=5$, $xy=6$).

$$\underline{\underline{E}} = \begin{pmatrix} E_{11} & E_{12} & E_{12} & 0 & 0 & 0 \\ E_{12} & E_{11} & E_{12} & 0 & 0 & 0 \\ E_{12} & E_{12} & E_{11} & 0 & 0 & 0 \\ 0 & 0 & 0 & E_{44} & 0 & 0 \\ 0 & 0 & 0 & 0 & E_{44} & 0 \\ 0 & 0 & 0 & 0 & 0 & E_{44} \end{pmatrix}$$

The following table gives some values of the Young's moduli of different materials with cubic crystal structure:

material	$E_{11} = E_{xxxx} (10^{10} \text{ N/m}^2)$	$E_{44} = E_{yzyz} (10^{10} \text{ N/m}^2)$	$E_{12} = E_{xxyy} (10^{10} \text{ N/m}^2)$
diamond	107.6	57.6	12.5
Fe	23.3	11.8	13.5
NaCl	4.9	1.3	1.3
Pb	5.0	1.5	4.2
Na	0.8	0.4	0.6

Tab. 2.1: Typical values of the Young's moduli for materials with cubic crystal structure.

Obviously, there are major differences between soft and hard materials, for example, Young's moduli for diamond and sodium differ by 2 orders of magnitude. It is striking that diamond and iron are almost identical in the Young's modulus E_{12} , but differ in E_{11} by a factor of 5. Sodium chloride and lead show remarkably similar Young's moduli E_{11} and E_{44} , but differ in E_{12} .

2.2 Velocity of Sound

To understand the dependence between the velocity of sound and the Young's modulus we have to concentrate on the propagation of the elastic deformation in a solid body. A simple model for a solid body is a one dimensional linear spring chain. An excitation of an infinite chain leads to the wave equation:

$$\frac{d^2 A}{dx^2} = \frac{\rho}{E} \cdot \frac{d^2 A}{dt^2}$$

where ρ denotes the density and E the Young's modulus of the material. With the approach for a linear wave (A : deflection, A_0 : amplitude):

$$A = A_0 e^{i(kx - \omega t)}$$

and the definition of the velocity of sound (k : wave number, λ : wavelength):

$$v = \frac{\omega}{k} \quad k = \frac{2\pi}{\lambda}$$

The dispersion relation is given by:

$$v^2 = \frac{\omega^2}{k^2} = \frac{E}{\rho}$$

Since the phase velocity v and density ρ are known, the Young's modulus E can be calculated. As already mentioned in the introduction, changes of external parameters, such as temperature and phase transitions occurring within the solid, can lead to changes in the Young's moduli and thus in the velocity of sound. In contrast to sound waves propagating in air, where the deflection is always longitudinal (parallel to the propagation direction), the propagation in solids can either be longitudinal or transverse. In our experiment we use ultrasonic waves which propagate in the $[110]$ direction of the sample. For transverse waves the deflection can either be parallel to the $[001]$ or to the $[1\bar{1}0]$ direction. Longitudinal waves oscillate in the propagation direction $[110]$. The relation between the Young's moduli and the velocities of sound in the appropriate directions are illustrated in the following table:

wave mode	displacement direction	velocity
longitudinal	$[110]$	$v_{110} = \sqrt{\frac{E_{11} + E_{12} + 2E_{44}}{2\rho}}$
transverse	$[001]$	$v_{001} = \sqrt{\frac{E_{44}}{\rho}}$
transverse	$[1\bar{1}0]$	$v_{1\bar{1}0} = \sqrt{\frac{E_{11} - E_{12}}{2\rho}}$

Tab. 2.2: Relation between the velocities of sound and the Young's moduli E_{11} , E_{12} , and E_{44} . The wave propagates in the $[110]$ direction.

By measuring the three velocities of sound (v_{110} , v_{001} , $v_{1\bar{1}0}$) it becomes possible to determine the three linear independent Young's moduli E_{11} , E_{12} , and E_{44} .

2.3 Ultrasound Attenuation

All previous calculations neglect the attenuation of the sound wave. Nevertheless such attenuation occurs in all solids during the transmission of a sound wave. The main reasons for this are:

1. Magnetostriction effects
2. Scattering at impurities within the atomic lattice
3. Scattering at phonons (quantized lattice vibrations)
4. Scattering at conduction electrons
5. Microscopic induction of eddy currents at magnetic domain walls

Although there are different damping effects occurring over a variety of temperature ranges, the entire loss is always exponentially dependent on the propagation distance of the wave:

$$A(x) = A_0 e^{-\alpha x},$$

where A_0 denotes the initial amplitude, and x the length of the transmission path. Knowing the amplitudes A_1, A_2 of the sound wave at two different positions x_1, x_2 the damping constant α can be calculated using:

$$\alpha = \frac{\ln\left(\frac{A_1(x_1)}{A_2(x_2)}\right)}{x_2 - x_1}$$

with a unit of $[\alpha] = \text{m}^{-1}$. In practice, the initial amplitude A_0 is not necessary for the calculation of the attenuation. Usually the attenuation is specified in $[\alpha] = \text{dB/m}$ and can be calculated by:

$$\alpha = \frac{20 \cdot \log\left(\frac{A_1(x_1)}{A_2(x_2)}\right)}{x_2 - x_1}$$

2.4 Aim of the experiment

The aim of the experiment is the investigation of the velocity of sound and the sound attenuation with respect to temperature and external magnetic field of a $\text{Fe}_{0.7}\text{Al}_{0.3}$ single crystal oriented in the $[110]$ direction. Therefore the sample temperature can be varied from 77K up to 300K and a magnetic field of up to 600mT can be applied. You will also get more experience using measurement devices, such as the digital oscilloscope and pulse/waveform generators and as well as seeing the importance of triggering such instruments correctly.

2.5 Magnetic properties of $\text{Fe}_{0.7}\text{Al}_{0.3}$

In this experiment a $\text{Fe}_{0.7}\text{Al}_{0.3}$ polycrystalline material is investigated. The growth of the crystal was done at the “Max-Planck Institut für Eisenforschung” in Düsseldorf (Bridgeman technique, MPI specification: $\text{Fe}_{0.7}\text{Al}_{0.3}$ / diameter 4cm / Nr.: Sm653). After fabrication it has been shaped by spark erosion into a small rod of a length of 9mm and a diameter of 6mm.

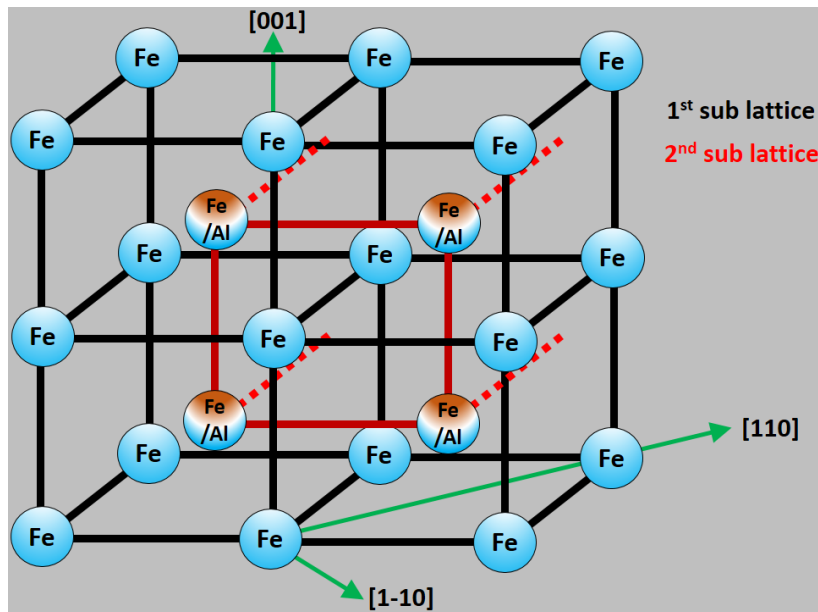


Fig. 2.3: Model of the lattice of the FeAl alloy. The three perpendicular lattice directions are indicated by the green arrows.

The grains of the Fe-Al alloy mostly crystallizes in a body cubic centered (bcc) lattice with two different superstructures. The $\text{Fe}_{1-x}\text{Al}_x$ lattice consists of two simple cubic sub lattices which are shifted against each other along the $[111]$ direction (see Fig. 2.3). If the crystal is cooled down very slowly during the preparation process the result is an ordered alloy. For an Al concentration of 25% the 2nd sub lattice has a NaCl structure, which means that Fe and Al atoms alternate regularly with a long range order. The quenched $\text{Fe}_{0.7}\text{Al}_{0.3}$ alloy does not have such a long range order, i.e., the Fe and Al atoms are randomly distributed over the 2nd sub lattice. In both cases the 1st sub lattice only consists of Fe atoms [1]. For Al concentrations >25% the additional Al atoms are randomly distributed over the 2nd sub lattice.

Fig. 2.4 shows the magnetic phase diagram of the $\text{Fe}_{0.7}\text{Al}_{0.3}$ alloy with respect to temperature. The phase diagram consists of paramagnetic, ferromagnetic, super paramagnetic, and spin glass states. For temperatures above the Curie temperature of $T_C = 400\text{K}$ the sample is in a paramagnetic state. Below T_C ferromagnetic order is established. In the range between $T_C^{\text{INV}} = 170\text{K}$ and $T_f = 92\text{K}$ the sample shows a mixed phase consisting of a super paramagnetic and spin glass ordered phase. Below T_f the sample is in the spin glass phase

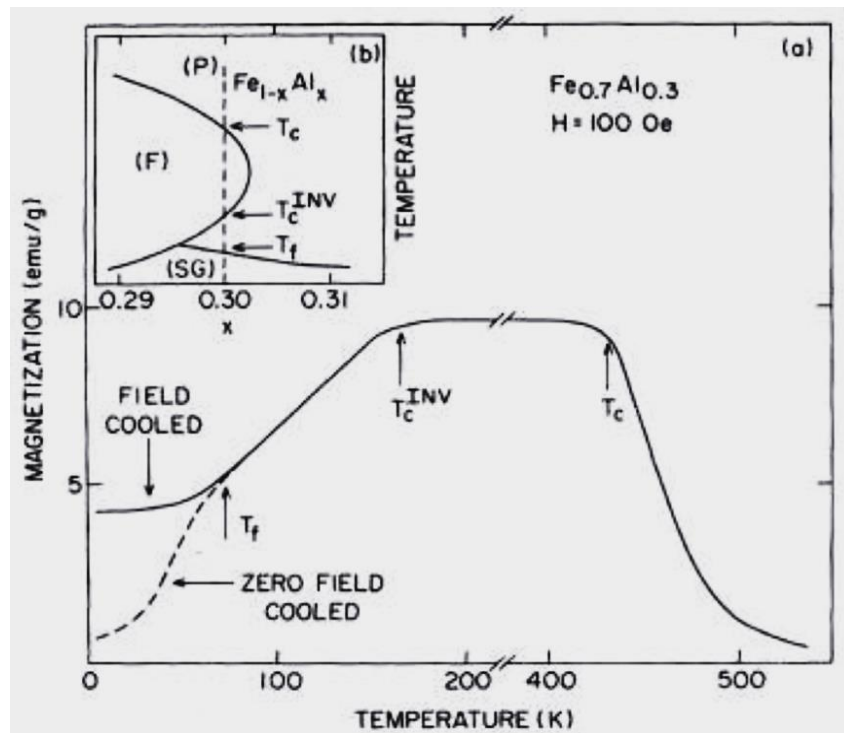


Fig. 2.4: Magnetic phase diagram of the FeAl alloy used in this experiment.

The following gives a short overview over the magnetic phases occurring in the FeAl sample:

1. **Paramagnetism:** The paramagnetic state shows no any spontaneous magnetization without an external field. The spin fluctuation is due to thermal energy. Applying an external field will align the spins parallel to the magnetic field direction
2. **Ferromagnetism:** The ferromagnetic state shows a spontaneous magnetization, i.e. with no external field applied. The spins are coupled by the exchange field and cluster into magnetically ordered regions, called magnetic domains. Within a magnetic domain all spins are aligned in the same direction. Applying an external magnetic field the domains will progressively align parallel to the field direction until full saturation is reached, i.e., only one big domain exists. For temperatures above the Curie temperature T_C the sample becomes paramagnetic.
3. **Antiferromagnetism:** In the antiferromagnetic state long range magnetic order is established, similar to the ferromagnetic phase. In contrast to ferromagnetism the exchange coupling does not align the spins into the same direction but with a certain angle between the spins. The most common antiferromagnetic order is the 180° alignment of neighbouring spins. The antiferromagnetic phase also shows magnetic domains, as for ferromagnetism, but no magnetization without an external field. Increasing the temperature above the Neel temperature T_N causes the material to go paramagnetic.
4. **Superparamagnetism:** The superparamagnetic phase is somewhat similar to the paramagnetic phase. Here, the magnetic domains are fluctuating due to the thermal energy and the spins within a domain are still aligned in the same

direction. This state has no spontaneous magnetization (no remnant magnetization in zero field). Applying an external magnetic field will align the fluctuating domains in the same spin direction.

5. **Spin glass state:** In the spin glass phase the spins point in randomly distributed directions, i.e., no magnetization exists at zero external field. In contrast to the paramagnetic phase the spins are not fluctuating but they are “frozen” in a certain direction. The reason for the formation of a spin glass phase are the competitive interaction forces between the Fe – Fe and the Fe – Al – Fe atoms. The Fe – Fe atoms favor a ferromagnetic coupling, while the Fe – Al – Fe atoms want to establish an antiferromagnetic order. This results in so called frustrated spins. Fig. 2.5 shows a frustrated spin marked by “F” which is aligned against the common spin matrix direction due to this competitive interaction forces. This “misaligned” spin direction also influences the neighboring spins again. If the number of frustrated spins is high enough, the order of the spins is totally destroyed, assuming the temperature is low enough. At only little higher temperatures parts of the collinear order already exists within the spin lattice.

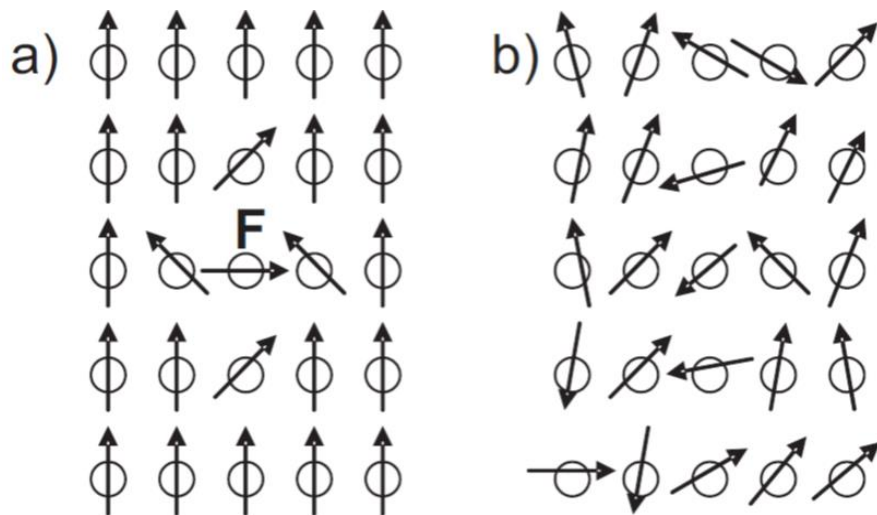


Fig. 2.5: Development of a spin glass phase. Spin matrix with a) one frustrated spin indicated by “F” and b) many frustrated spins.

In the following table further important properties of the cylindrical Fe_{0,7}Al_{0,3} sample are given [3,4]:

Property		Fe _{0,7} Al _{0,3} Sample
Length	(mm)	9.191
Diameter	(mm)	6.014
Weight	(g)	1.6996
Density	(kg/m ³)	6510
E ₁₁	(10 ¹⁰ N/m ²)	16.83
E ₄₄	(10 ¹⁰ N/m ²)	13.10
E ₁₂	(10 ¹⁰ N/m ²)	11.85

Tab. 2.3: Properties of the Fe_{0,7}Al_{0,3} alloy.

3 Experimental Setup

Fig. 3.0 shows a photograph of the experimental setup. The sample is located in the center of the yoke of the electromagnet. The whole sample holder is inserted into a stainless steel tube, which can be evacuated or filled with helium gas. This inner tube is fixed in the liquid nitrogen cryostat (insulated glass fiber reinforced tube). In the upper part of the setup electrical feedthroughs for high frequency signals, thermal sensor and heating are installed. In addition valves on the side and rear allow pumping and venting the system with helium exchange gas.

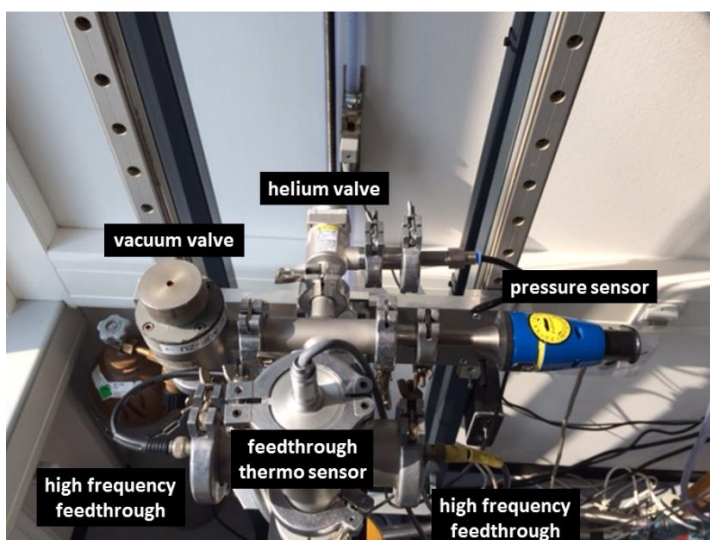
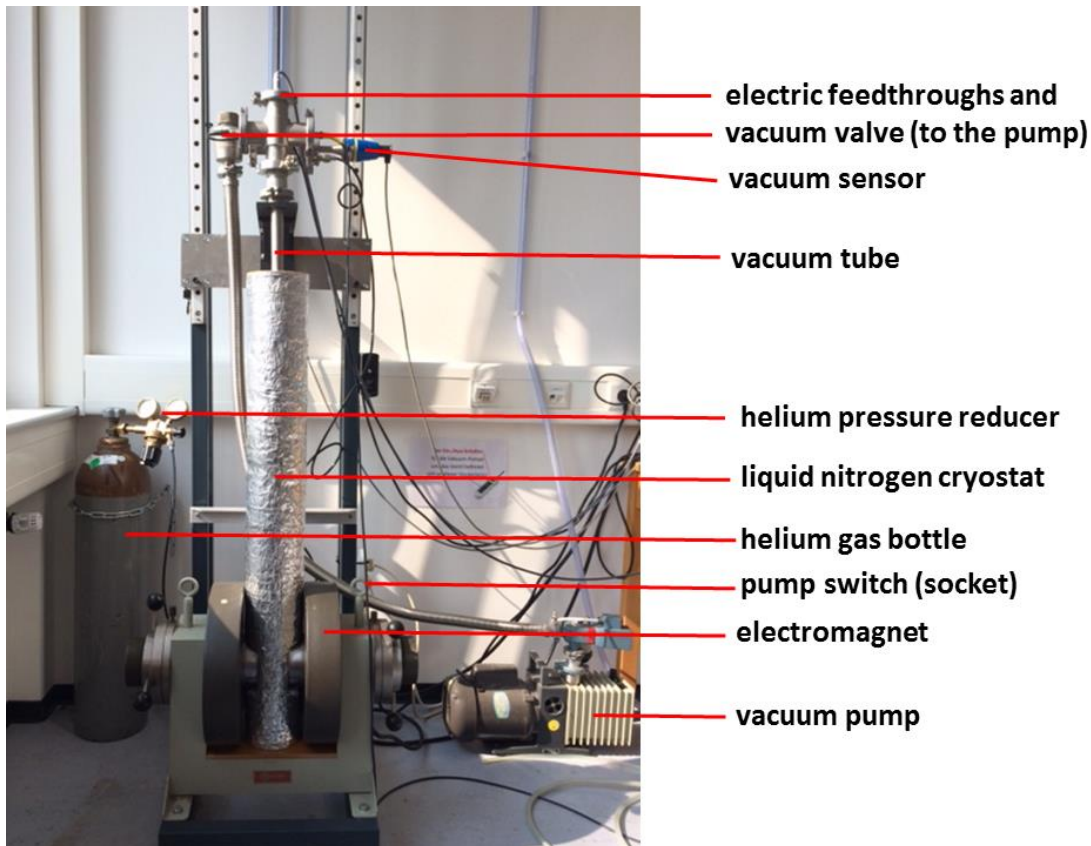


Fig. 3.0: Photographs of the experimental setup.

3.1 The Sample Holder

The sample holder is illustrated in Fig. 3.1. This sample holder is mounted in a stainless steel tube which can be evacuated and filled with helium gas to ensure good thermal contact of the sample and the wall of the tube. This tube is inserted into a second glass fiber reinforced plastic tube, containing liquid nitrogen in order to cool down the whole system to 77K. When warming the sample the inner tube is evacuated again to reduce the cooling power from outside and additionally manganin heating coils can be switched on.

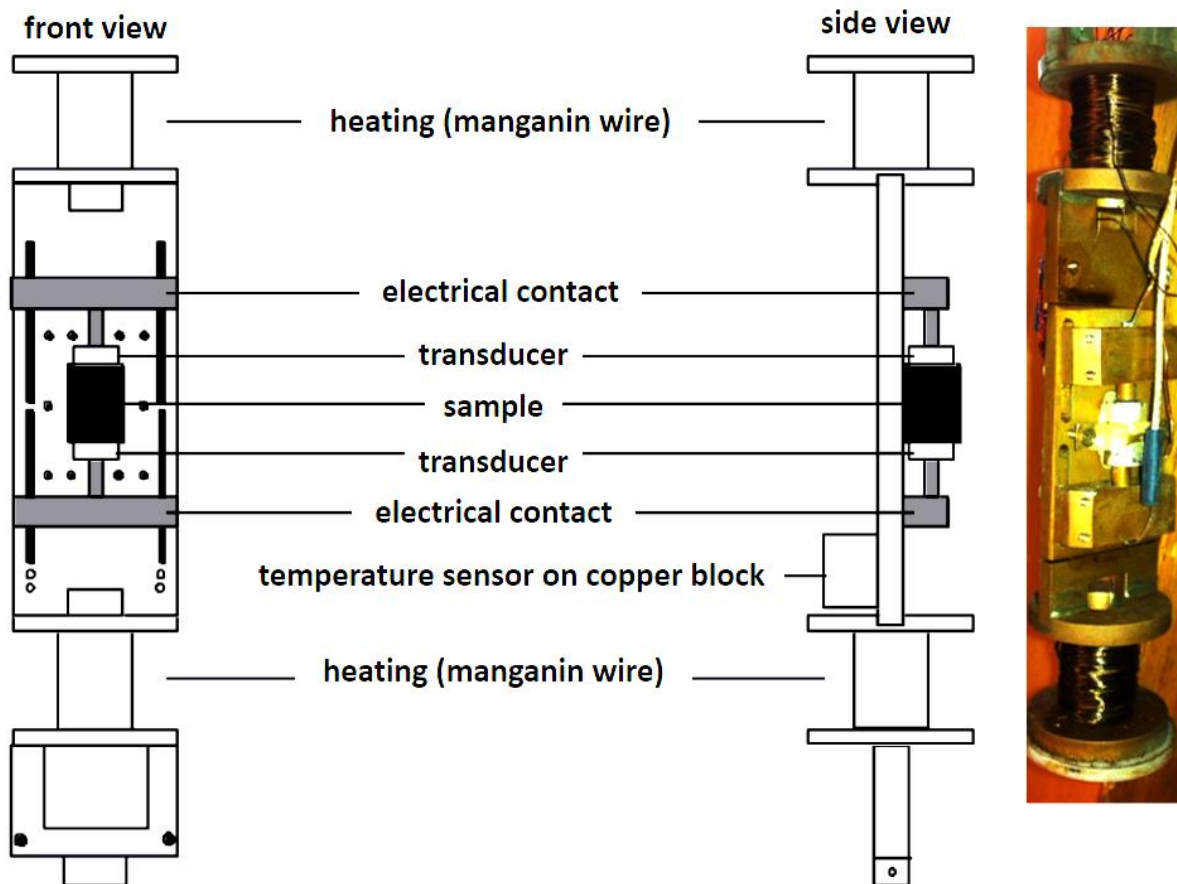


Fig. 3.1: Sketch and photograph of the sample holder.

3.2 Determining the temperature

To measure the temperature during the measurement a sensor (PT-102) is mounted near the sample (see Fig. 3.1). The measurement electronics determine the resistance of the sensor which is temperature dependent. To remove parasitic resistance of the cables the measurement is done by the “four point method”. This means one pair of cables is connected across the sensor providing a constant current with the other two cables are connected in parallel to the first pair to measure the resulting voltage. The connectors at the electronics (“Ultraschallmessgerät”) labelled “I” (output) and “U” (input) are located on the rearside. On the front side the current can be chosen by a five-way selector switch ($I = 0.01\text{mA} / 0.1\text{mA} / 1\text{mA}$). The

value you want is $I = 0.1\text{mA}$. An open current circuit is indicated by the red LED near the current selector. Note that the small toggle switch at the rear of the electronics must be in the position “Rück”.

During sample warming-up, every 20K a thermal voltage compensation must be performed in order to get rid of an additional thermal voltage induced in the cables. This can be done via the following procedure:

1. Switch off the current by selecting the position “0” on the current selector switch. Now the thermal voltage is indicated by the display.
2. Press the button “dU” until a “Δ” appears at the display and the thermal voltage changes to 0mV.
3. Switch on the appropriate current again by the selector switch to return to the temperature measurement.

The temperature can be displayed in °C or K which can be chosen by an additional toggle switch near the display. Fig. 3.2 shows the front panel of the measurement electronics.



Fig. 3.2: Ultrasound measurement electronics. The parts used for the temperature measurement are marked in red.

The two manganin coils (sample heater) can be heated up by a current (**maximum 300mA**) which is applied with an external power supply and measured by a digital ammeter.

3.3 The Ultrasound transducer

Ultrasound transducers are fabricated from piezo electric materials, e.g., SiO_2 (quartz), BaTiO_3 and LiNbO_3 . The material is cut into small circular plates and coated with silver or gold to form electrodes on both sides. The small plates (diameter of 3.5mm) are then glued to both ends of the FeAl sample rod. Mechanical deformation of a piezo electric material causes a change in the relative distance of positive and negative ions within the atomic lattice, thus resulting in a voltage drop along a polar axis. The application of a voltage to a piezo electric material induces a mechanical deformation, which is called the inverse piezo electric effect. Using an ac-voltage a

mechanical oscillation of the transducer can be generated. Depending on the crystal orientation of the transducer material the oscillation can be perpendicular or parallel to the surface of the transducer, thus inducing either a longitudinal or a transversal ultrasound wave. The transducers can be used to both introduce an ultrasonic wave into the sample and also to detect the sound wave. To increase the amplitude of the mechanical oscillation the exciting frequency should be set closely to the resonance frequency of the transducer. The resonance frequency is given by the thickness and density of the transducer material. In our experiment we use BaTiO_3 transducer plates with a thickness of about 0.2mm resulting in a resonance frequency of 10MHz. To ensure good mechanical coupling between the transducer plate and the sample the transducer is glued by a conductive epoxy glue to both ends of the FeAl sample rod.

3.4 The External Magnetic Field

A magnetic field can be applied with an electromagnet (manufacturer: Varian), which should only be operated with a functioning cooling watersystem. The power supply (Delta Elektronik SM 300-100D) provides up to 65A for the magnet. The power supply will be switched on by the supervisor of the experiment. If the cooling water is switched off, no current can be applied due to an interlocked flow sensor. The magnetic field B with respect to the applied current is shown in the calibration diagram (see Fig. 3.2).

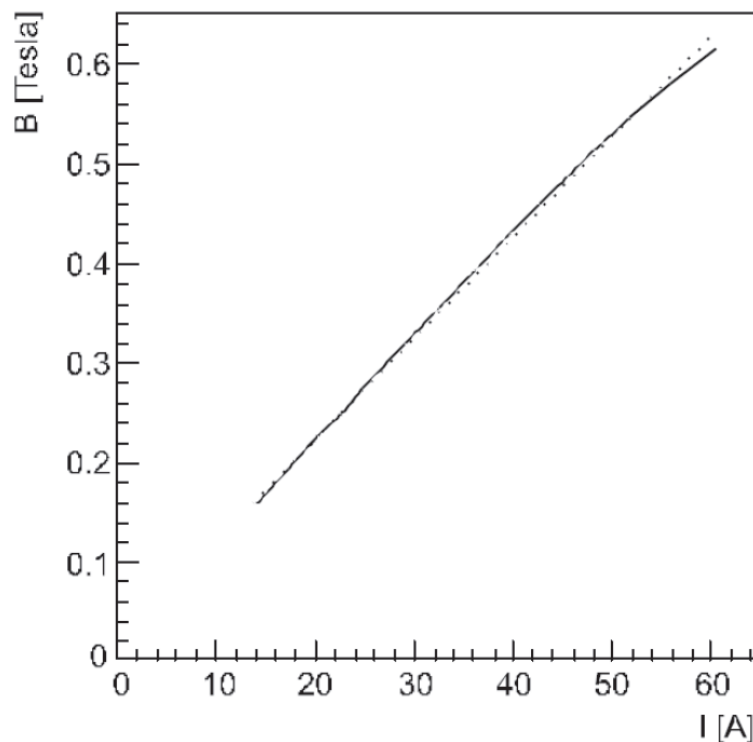


Fig. 3.3: Magnetic field B with respect to the applied current I of the electro-magnet. Solid line: data, dotted line: linear fit to data.

The calibration has been done with an NMR sensor (nuclear magnetic resonance sensor). As shown in Fig. 3.3 the calibration curve can be approximated by a linear fit:

$$B = B_0 + b \cdot I$$

Where $B_0 = 0.0207$ T is a small field offset due to the remanent magnetization of the yoke and $b = 0.0102$ T/A is the slope of the curve.

3.5 Electronic Setup: Pulse Echo Overlap Method

The determination of the ultrasound velocity and attenuation will be done by the so called “pulse echo overlap method”. A schematic of the measurement electronics is shown in Fig. 3.4. The pulse modulator (Wavetek Model 191 function generator) generates a 10MHz sinusoidal wave packet. The length of the wave packet can be adjusted at the pulse modulator (selector switch “pulse width/burst width”). It turns out that a wave packet containing 3 - 5 maxima is a good choice. The start of one wave packet will be triggered by a square pulse at the input “trigger in” of the Wavetek generator. Therefore the selector switch “mode trig level” should be set to “burst trig”. The inner potentiometer dial of the selector sets the trigger level. Note that the trigger only works over a very small potentiometer range. At the “func out” BNC connector, the resulting wave packet can be measured. This wave packet is amplified by the HF amplifier. Note that **the input signal must not be larger than 1V!** The output of the amplifier is directly connected to the ultrasound transducer within the cryostat (BNC cable to the upper feedthrough of the apparatus). The ultrasonic wave enters the sample rod and is measured on the other side by a second transducer, which converts the mechanical wave back into a voltage. This voltage signal can be amplified (amplifier integrated in the “Ultraschallmessgerät”) or be measured directly by the digital oscilloscope.

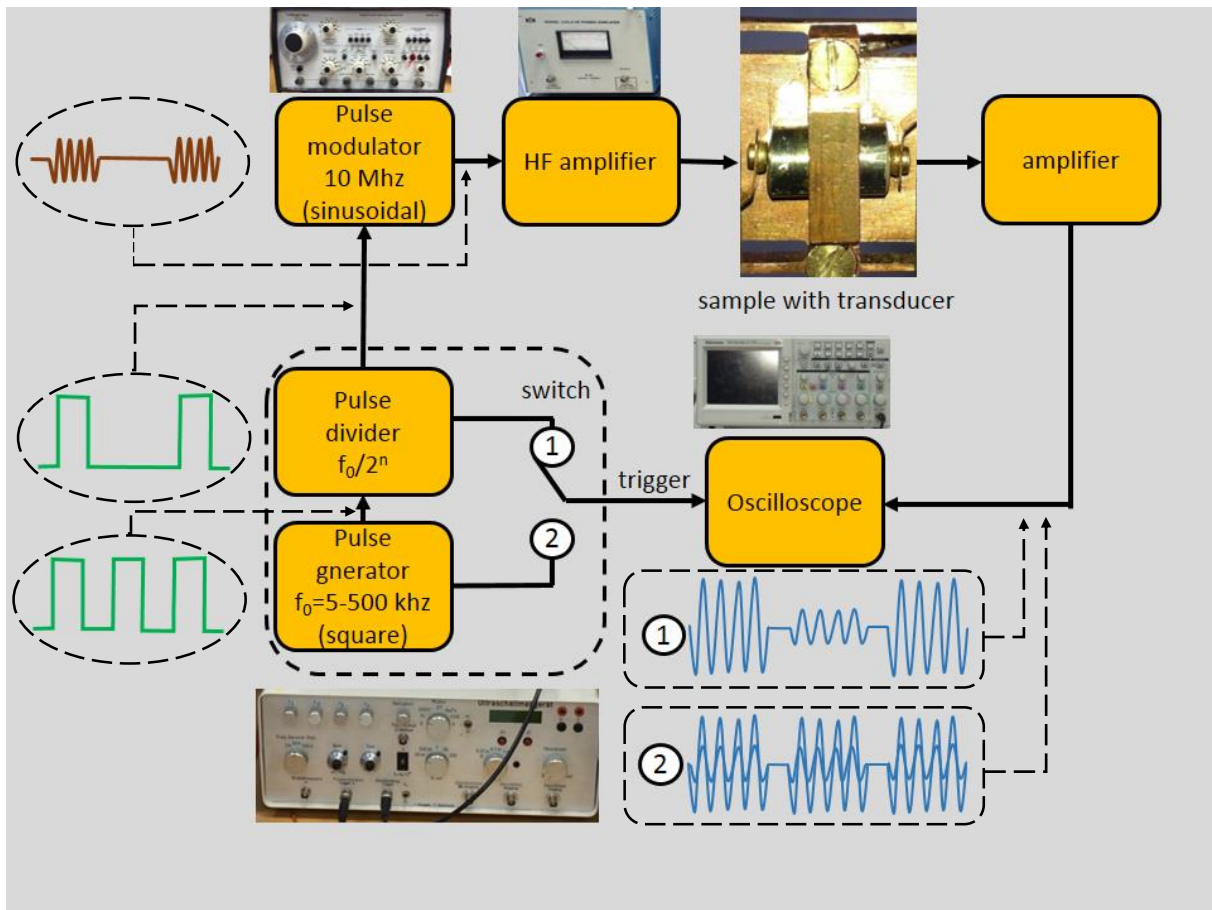


Fig. 3.4. Schematic of the setup used to measure the ultrasound velocity and attenuation by the “pulse echo overlap method”.

A part of the ultrasonic wave is reflected at the ends of the sample. The echo will also enter the second transducer after a time Δt with a smaller amplitude due to the damping. To determine the velocity of sound the time between the transmitted wave package and the first echo must be measured. The velocity of sound can easily be calculated by:

$$v = \frac{2L}{\Delta t}$$

where L denotes the length of the sample. To measure the time Δt by the oscilloscope the time distance between one maximum of the transmitted wave package and the related maximum of first echo can be determined by the cursor function of the oscilloscope. The only problem applying this method is a relatively large error because the time distance between the wave packages is much larger than the period time of the sinusoidal wave within the package. Measuring the distance with the cursors on the screen of the oscilloscope is only possible by zooming out so that both packages are visible.

The “pulse echo overlap method” is more accurate because the transmitted pulse and first echo is drawn simultaneously at the same position on the screen of the oscilloscope. Therefore the number of square pulses triggering the pulse modulator are reduced by the pulse divider. The new frequency f_1 is given by:

$$f_1 = \frac{f_0}{2^n}$$

Choosing a number of $n = 1$ at the selector, i.e., every second square pulse is sent to the trigger input of the pulse modulator. Selecting $n = 2$ means only every fourth pulse is sent, etc. We will learn that the chosen number n is equivalent to the number of expected echoes. But how do you show the two wave packages overlapping on the oscilloscope? The square pulses from the pulse generator are trigger not only the pulse modulator but the oscilloscope as well. A signal applied to the trigger input of the oscilloscope starts a single shot measurement of the input signal. Therefore the record length should be given by the chosen time base of the oscilloscope, i.e., triggering the oscilloscope by the undivided frequency f_0 the single shot measurements are repeated at exactly this frequency. If now f_0 is adjusted in such a way that the time difference Δt between the transmitted wave package and its first echo is given by:

$$\Delta t = \frac{1}{f_0}$$

then the initial wave package is superimposed with the first echo from the preceding pulse and it becomes difficult to measure a reasonable signal. Therefore only every second wave package ($n = 1$) is sent to the sample, but the oscilloscope is still taken single shot measurements with f_0 , i.e., the first shot measures the initial signal, the second shot measures the first echo, etc. This results in an almost simultaneous presentation of initial wave and first echo on the screen of the oscilloscope. Now it is easy to adjust the position of the maxima of the two signals by adjusting the frequency f_0 . The velocity of sound can be calculated by:

$$v = 2Lf_0$$

The trigger frequency of the oscilloscope is directly measured and indicated on the screen. An additional toggle switch at the pulse generator allows triggering the oscilloscope either on f_0 or f_1 . Using f_1 as a trigger signal, the transmitted wave package and the echo is no longer displayed simultaneously, because every second shot is left out. Due to the divided frequency the initial wave and the first echo are shown one after the other on the screen (real time). To clarify this Fig. 3.5 shows two examples for $n = 1$ (only one echo) and $n = 2$ (two echoes of the initial signal) and the appropriate curves displayed by the oscilloscope for different trigger signals. Note that the number n must be adjusted to the absolute number of echoes, otherwise a superposition of two or more echoes can occur.

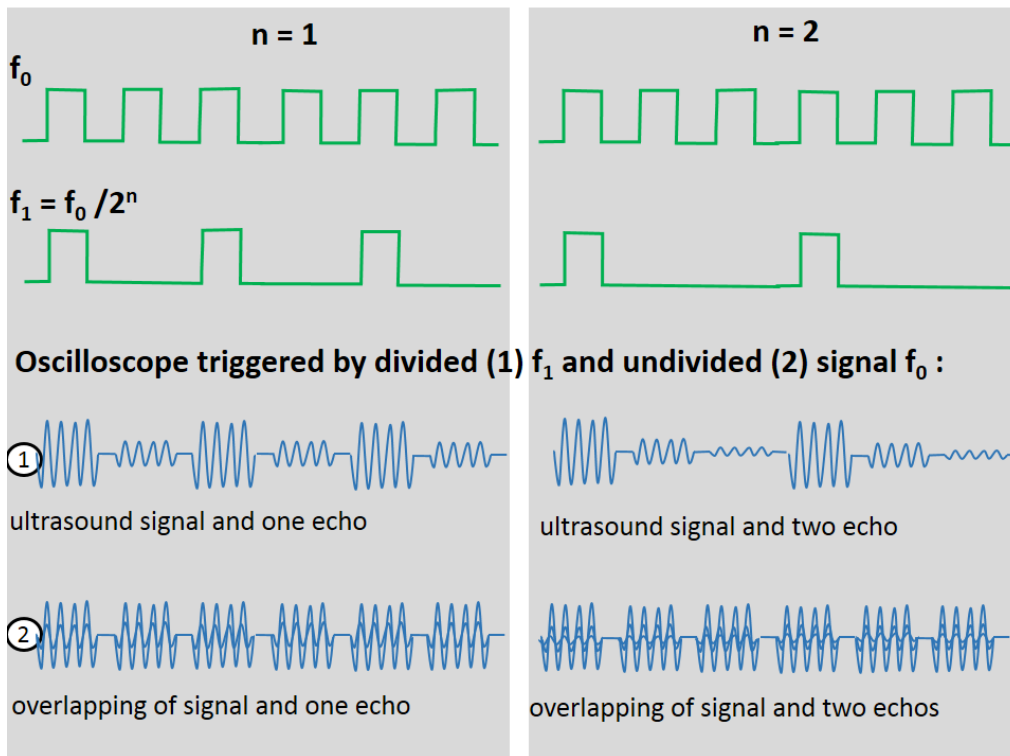


Fig. 3.5: Example for a measurement of one and two echoes of the ultrasound signal. The pulse modulator is always triggered by the divided frequency f_1 and the oscilloscope is triggered either by f_0 (pulse overlap method) or by f_1 (regular measurement).

3.5 Estimation of Errors

The errors which have to be considered are given on the one hand by the resolution of the oscilloscope (Δf , ΔT) and the possible accuracy in overlapping the maxima of wave and echo. On the other hand the dispersion of the wave package has to be taken into account, i.e., the wave package diverges on the way through the sample. This error can be determined by overlapping the first maximum of the wave package with its echo. The time difference between the last maximum and its echo determines the error. Fig.3.6 illustrates this.

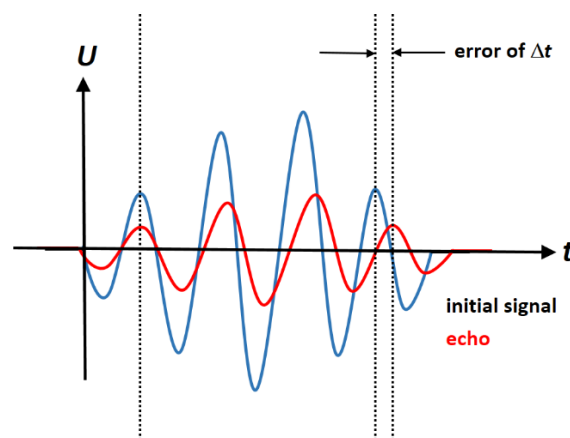


Fig. 3.6: One method of determining the error of Δt due to the dispersion of the wave package.

You may assume an error of the sample length of $\Delta L = 10\mu\text{m}$ the error of the velocity of sound results, following the Gaussian error propagation, in:

$$\Delta v = \sqrt{(2f_0 \cdot \Delta L)^2 + (2L \cdot \Delta f_0)^2}$$

or

$$\Delta v = \sqrt{\left(\frac{2}{\Delta t} \cdot \Delta L\right)^2 + \left(\frac{2L}{\Delta t^2} \cdot \Delta(\Delta t)\right)^2}$$

3.6 Determination of the Sound Attenuation

Measuring the ultrasound attenuation can also be performed by the method described in chapter 3.5, but now the peak-to-peak amplitude of one maximum and the echo are compared. This measurement can be done more easily with a modified measurement circuit. An additional rectifier and a downstream low pass filter which are integrated in the “Ultraschallmessgerät”, are used after the amplifier (“Gleichrichter” output). This leads to a pulse shaping such that the envelope of the wave package is formed (see Fig. 3.7). The resulting amplitude of the curve can be compared to the echo

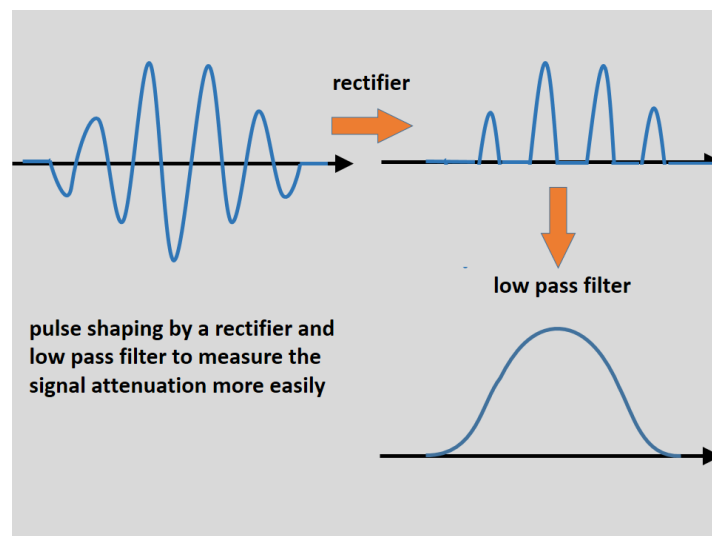


Fig. 3.7: Pulse shaping using a rectifier and a low pass filter.

4 Physical Background

This chapter goes through a short summary of the physical effects related to ultrasound application and measurement.

4.1 Magnetostriction Effect

Magnetostriction describes a change in geometry, e.g., the strain $\Delta L/L$ of a solid body induced by an external magnetic field. There are two types of magnetostriction

effects. Normally the volume of the solid stays constant during an elastic strain induced by a magnetic field. This is called Joule magnetostriction. If the magnetostriction is accompanied by a change of the volume, the effect is called volume magnetostriction. This effect is observed for invar alloys and is much smaller than the Joule magnetostriction. The value of the volume magnetostriction is positive if the configuration with the larger volume corresponds to the configuration with the larger magnetization. In case of Joule magnetostriction the sign depends on whether the material is extended (positive) or compressed (negative) along the magnetization direction. Typical values are $\Delta L/L=10^{-8}$ to 10^{-3} in case of magnetic saturation. The reason for the macroscopic magnetostriction is the aligning of the magnetic moments with the applied external field. This results in a change of the atomic bonding lengths due to the spin orbit coupling and thus in a change of the sample geometry. As already described in chapter 2.5 a ferromagnetic material consists of many magnetic domains, i.e., areas with the same direction of the spins. The magnetization direction of the different domains are statistically distributed (in the case that no magnetic anisotropy is present) and no average magnetic magnetization of the whole sample can be measured (demagnetized state). The transition regions between two magnetic domains, where the spins rotate from one to the other direction, are called domain walls. Depending on the rotation plane of the spins the domain walls are called “Bloch walls” or “Néel walls”. For thick samples Bloch walls are favored because of the reduced stray field energy. The domain walls are further characterized by the angle between the two neighboring domains, e.g., domain walls between two antiparallel aligned domains are called 180° -domain walls. Fig. 4.1 illustrates the rotating spin directions within 180° domain walls. The magnetic domains are responsible for the magnetostriction effect. In case of a demagnetized ferromagnetic state the atomic lattice is deformed due to the different magnetization directions of the domains. When applying an external magnetic field, a change of the domain structure is induced and thus a changing deformation of the lattice. This effect is maximal if all domains are aligned parallel to the external field (magnetic saturation) and the lattice is stretched or compressed along this direction. In addition, the magnetostriction influences the stiffness (Young’s modulus) of the material and thus the velocity of sound.

The relative change of ΔE can be determined by measuring the velocity of sound with (E_B) and with no ($E_{B=0}$) applied external magnetic field. The relative change of the Young’s modulus is called ΔE -effect:

$$\frac{\Delta E}{E_B} = \frac{E_B - E_{B=0}}{E_B} = 1 - \frac{E_{B=0}}{E_B}$$

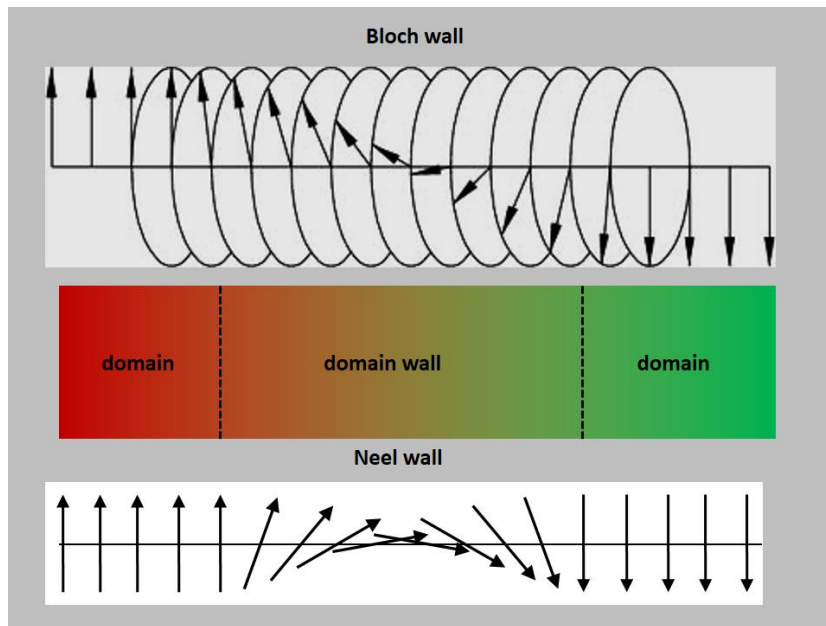


Fig. 4.1: Types of magnetic domain walls (180° domain walls).

4.2 Ultrasound Attenuation

As previously mentioned in chapter 2.3 the damping of the ultrasound wave propagating through a solid material has a number of causes:

1. **Damping by magnetostriction:**

The ultrasound wave induces an oscillation of the atomic lattice which leads to a small change in the local magnetization (magnetic domains are slightly shifted towards each other). This results in a local change of the lattice spacing thus inducing friction and heat losses.

2. **Damping by microscopic eddy currents:**

The lattice oscillation induced by the propagating ultrasound wave change the local magnetization at the domain walls and thus a local change of the internal magnetic stray field. The changing magnetic field induces eddy currents which are damped by the sample resistance, i.e., heating up the lattice. This effect depends on the number of magnetic domain walls within the sample.

3. **Damping by phonons**

The heat energy of a crystal is stored in quantized lattice vibrations, i.e., phonons. A sound wave is a coherent packet of phonons partly scattered by the thermal phonons. Considering the ultrasound wave as a flow of monochromatic phonons with relatively low energy, the effect can be described as a phonon-phonon interaction. The energy of the coherent sound wave is diminished leading to an increase of the thermal energy (temperature) of the material. Note that the measured damping with an applied saturation field (no damping by magnetic domain walls any more) can be mostly attributed to the phonon damping.

4. **Damping by electrons:**

Conductive materials contain free electrons which are distributed over the whole lattice (free electron gas). Although they provide only little contribution to the specific heat of the crystal, their contribution to the heat conductance is considerable. A lattice oscillation induced by the sound wave leads to a local shift of the positive charged atomic cores against the free electrons. Therefore the distribution of the electron velocity is continuously changing. This effect scales with the frequency of the sound wave. Relaxation of this electronic distribution leads to the damping effect. In the experiment the damping by electrons is a fixed offset (temperature independent) of the attenuation. Distinguishing between damping effects induced by phonons and electrons can only be made at very low temperatures in order to freeze out all phonons.

5. Experimental Procedure

5.1 Experimental Procedures and Tasks

The experiment should be performed in the following order. Parts shown in green should be done at home during the preparing of the protocol:

1st day:

1. Connecting and testing of the electronic components according to the scheme in Fig. 3.4. The signals should be checked by the 4-channel digital oscilloscope. It should be possible to measure the velocity of sound in “regular” mode and with the “pulse echo overlap” method. This part of the experiment is intended to build familiarity with the measurement setup up and the trigger logic (2 – 3 hours).
2. Determination of the velocity of sound at room temperature ($T = 300\text{K}$) by the two different methods described before.
3. Compare the resulting errors of the velocity regarding the two different methods (measurement of Δt by the cursors and f_0 by the pulse echo overlap method).
4. How large is the error concerning the pulse dispersion?
5. Is the experiment carried out with a longitudinal or a transversal ultrasound wave? (Tip: check typical values for the sound velocities of longitudinal and transversal waves for the used elements).
6. Calculate the Young’s modulus E_{44} . Note that the relation between the velocity and E_{44} depends on the oscillation direction of the wave. Unknown parameters are given in previous tables. Compare the calculated value with the literature value of E_{44} (see table).
7. Measurement of the sound attenuation at room temperature including error determination.
8. Determination of the velocity of sound and the attenuation with respect to an external magnetic field at room temperature. Measure from $B = 0\text{T}$ until saturation is reached (step size 1A; **maximum of magnet current: 50A**). How large is the saturation field B_s ?
9. Plot the data graphically (attenuation in units of dB/cm, magnetic field in units of T, don’t forget error bars). Discussion of the resulting curves!
10. Cool down the sample to $T < 85\text{K}$ with liquid nitrogen (LN_2).

11. Measure the velocity of sound by the two methods and compare the values again.
12. Measurement of the sound attenuation.

2nd day:

1. Determination of the velocity of sound and the attenuation with respect to an external magnetic field at liquid nitrogen temperature. Measure from $B = 0\text{T}$ until saturation is reached (step size 1A; **maximum magnet of current: 50A**).
2. Plot the data graphically (attenuation in units of dB/cm, magnetic field in units of T, do not forget error bars). Discussion of the resulting curves. Compare the results to the curves measured at room temperature → discussion!
3. Measurement of the sound velocity and attenuation with respect to the temperature (from $< 85\text{K}$ to 300K). The step size should be small enough ($\sim 2\text{K}$) in the range of the expected magnetic phase transitions. This measurement should be done with and without magnetic saturation field B_s .
4. Plot the data graphically (with error bars). Discussion of the curves regarding magnetic phase transitions, temperature dependent damping effects, etc.
5. Calculate the relative change of the Young's modulus E_{44} with respect to temperature (ΔE effect):

$$\frac{\Delta E^{44}}{E_B^{44}} = 1 - \frac{E_{B=0}^{44}}{E_B^{44}}$$

and plot the data graphically. Discussion of the curve.

5.2 Cooling Down the System

Note that the following steps should be **monitored by the supervisor**:

- Switch on the vacuum pump (switch at the multiple socket). After 1 min. open the valve at the upper part of the system.
- Switch on the pressure sensor and wait until a pressure smaller than $5 \cdot 10^{-2}$ mbar is indicated.
- Close the valve at the upper part of the system again.
- Open the helium gas bottle and choose a very small pressure at the pressure reducer.
- Open the second valve at the upper part of the system in order to admit helium gas.
- Switch off the pressure sensor.
- Close the valve after 30 seconds again.
- Switch of the pump.

- Fill the cryostat carefully with liquid nitrogen. For safety reasons **wear gloves and protective goggles.**
- Check the filling level of the cryostat from time to time and refill if necessary.

5.3 Warming Up the System

To warm up the sample slowly during the measurement, please be aware of the following steps:

- Switch on the pump and the pressure sensor.
- Open the valve to the pump mbar in order to remove the exchange gas (helium). Do not switch off the pump until the cryostat is at room temperature again.
- Switch on the sample heater controlling the heater current. The current **may not extend 300mA.**
- After the measurement switch off the heater, close the valve and switch off the vacuum pump (should also be **controlled by the supervisor**).
- **Please note that switching off the pump without closing the valve will vent the system with air. This can lead to a destruction of the inner setup because of the freezing and expanding water (air humidity).**

5.4 General Safety Instructions

- During handling liquid nitrogen and dewars **protective goggles and gloves** has to be used.
- **The current of the electromagnet may never exceed 65A!**
- The handling of the glass dewars must be careful (danger of splintering).
- The heating current may not exceed 300mA.
- The input voltage of the HF amplifier must not exceed 1V.
- **Never vent the cold cryostat to air!**

6. Literature

- [1] Spin-glass behavior in iron-aluminum alloys: A microscopic model. Phys. Rev. B 21 159 (1980).
- [2] Neutron scattering studies of the anomalous magnetic alloy Fe_{0.7}Al_{0.3}. Phys. Rev. B 28 6183 (1983).
- [3] Messung der Schallgeschwindigkeit und Dämpfung an Fe_{0.7}Al_{0.3}-Einkristallen zwischen 300 K und 4,2 K. Diplomarbeit von U. Czubayko, Institut für Metallkunde und Metallphysik, RWTH Aachen (1990).
- [4] K.-H. Hellwege: Landolt-Börnstein, Zahlenwerte und Funktionen. Band III, Springer-Verlag, Berlin (1969).
- [5] M. Kersten: Zur Deutung der mechanischen Dämpfung ferromagnetischer Werkstoffe bei Magnetisierung. Zeitschrift für technische Physik, 463 (1934).
- [6] R.Becker, W.Döring: Ferromagnetismus. Springer-Verlag, Berlin, (1939).
- [7] C.Kittel: Physical Theory of Ferromagnetic Domains. Rev. Mod. Phys. 21, 541 (1949).
- [8] W.P.Bozorth: Ferromagnetism. D.van Nostrand Company, Princeton New Jersey Toronto London New York (1951).
- [9] C.Zener: Internal Friction in Solids: V.General Theory of Macroscopic Eddy Currents. Physical Review 53, 1010 (1938).
- [10] E.Kneller: Ferromagnetismus. Springer-Verlag, Berlin (1962).
- [11] G.T.Rado, H.Suhl: Magnetism. Band I-V, Academic Press, New York (1963).
- [12] M. Sparks: Ferromagnetic-Relaxation Theory. McGraw-Hill Comp., New York San Francisco Toronto London (1964).
- [13] J. Gleitzmann: Untersuchungen zur Abscheidung texturierter hochmagnetostriktiver TbDyFe-Schichten. Dissertation, TU Braunschweig (2000).
- [14] Mechanische Spektroskopie an Eisen-Aluminium und an Polymerschichten. Dissertation von A. Nagy, Gemeinsamen Fakultät für Maschinenbau und Elektrotechnik der Technischen Universität Carolo-Wilhelmina zu Braunschweig (2002).
- [15] H. Kuttruff: Physik und Technik des Ultraschalls. S. Hirzel Verlag Stuttgart (1988).